Multiphase sulfur chemistry facilitates particle growth in a cold and dark urban environment

Journal:	*Faraday Discussions*
Manuscript ID	FD-ART-10-2024-000170
Article Type:	Paper
Date Submitted by the Author:	18-Oct-2024
Complete List of Authors:	Mao, Jingqiu; University of Alaska Fairbanks, Department of Chemistry and Biochemistry & Geophysical Institute Bali, Kunal; University of Alaska Fairbanks, Department of Chemistry and Biochemistry & Geophysical Institute Campbell, James; University of Alaska Fairbanks, Robinson, Ellis; Johns Hopkins University, Department of Environmental Health and Engineering DeCarlo, Peter; Johns Hopkins University, Department of Environmental Health and Engineering Ijaz, Amna; Aix-Marseille Universite Temime-Roussel, Brice; Aix-Marseille Université, Sciences Barbara, D'Anna; Aix-Marseille Université Ketcherside, Damien; University of Montana Missoula, Chemistry and Biochemistry Yokelson, Robert; University of Montana, Chemistry Hu, Lu; University of Montana, Cesler-Maloney, Meeta; University of Alaska Fairbanks, Chemistry & Biochemistry; University of Alaska Fairbanks, Geophysical Institute Simpson, William; University of Alaska Fairbanks, Chemistry & Biochemistry Guo, Fangzhou; University of Houston System; Aerodyne Research Inc Flynn, James; University of Houston St. Clair, Jason; NASA Goddard Space Flight Center; University of Maryland Baltimore County Nenes, Athanasios; EPFL, Weber, Rodney; Georgia Institute of Technology

SCHOLARONE™
Manuscripts

Multiphase sulfur chemistry facilitates particle growth in a cold and dark urban environment

Jingqiu Mao, Kunal Bali, James Campbell,
Geophysical Institute and Department of Chemistry and Biochemistry, University of Alaska Fairbanks, Fairbanks, AK, USA

Ellis Robinson, Peter DeCarlo
Department of Environmental Health and Engineering, John Hopkins University, Baltimore, Maryland 21218, United States

Amna Ijaz, Brice Temime-Roussel, Barbara D'Anna,
Aix Marseille Univ, CNRS, LCE, Marseille, France

Damien Ketcherside, Robert J. Yokelson, Lu Hu,
Department of Chemistry and Biochemistry, University of Montana, Missoula, MT 59812, USA

Meeta Cesler-Maloney, William Simpson,
Geophysical Institute and Department of Chemistry and Biochemistry, University of Alaska Fairbanks, Fairbanks, AK, USA

Fangzhou Guo, James H. Flynn
Earth & Atmospheric Sciences, University of Houston, Houston, TX 77204, USA
Now at: Aerodyne Research Inc, Billerica, MA 01821

Jason St. Clair
Atmospheric Chemistry and Dynamics Laboratory, NASA Goddard Space Flight Center, Greenbelt, Maryland 20771, United States; Joint Center for Earth Systems Technology, University of Maryland Baltimore County, Baltimore, Maryland 21228, USA

Athanasios Nenes,
School of Earth and Atmospheric Sciences, Georgia Institute of Technology, Atlanta, Georgia 30332, United States
Laboratory of Atmospheric Processes and their Impacts, School of Architecture, Civil and Environmental Engineering, École Polytechnique Fédérale de Lausanne, Lausanne 1015, Switzerland
Center for the Study of Air Quality and Climate Change, Institute of Chemical Engineering Sciences, Foundation for Research and Technology Hellas, Patras 26504, Greece

Rodney Weber
School of Earth and Atmospheric Sciences, Georgia Institute of Technology, Atlanta, Georgia 30332, United States

Correspondence to: Jingqiu Mao (jmao2@alaska.edu), Kunal Bali (kbali@alaska.edu) and Ellis Robinson (esrobinson@arizona.edu).

Abstract

Sulfate comprises an average of 20% of the ambient $PM_{2.5}$ mass during the winter months in Fairbanks, based on 24-hour filter measurements. During the ALPACA 2022 field campaign (Jan

15th-Feb 28th of 2022), we deployed two aerosol mass spectrometers (AMS) and one aerosol chemical speciation monitor (ACSM) at three urban sites, combined with Scanning Mobility Particle Sizers (SMPS), to examine the evolution of aerosol composition and size distribution at a sub-hourly time scale. During an intense pollution episode with ambient temperature between -25 and -35°C, all three instruments (two AMS and one ACSM) recorded a sharp increase in sulfate mass, ranging from 5 to 40 μg/m³ within a few hours. This increase contributed up to half of the observed rise in ambient $PM_{2.5}$ mass concentration and coincided with a substantial shift in the number distribution from particle sizes less than 100 nm diameter ($D_p < 100$ nm) to larger particles ($D_p > 100$ nm) with little increase in number concentration. The corresponding increase in the volume concentration and distribution shift to larger particle size suggests the secondary formation of sulfate and organic aerosol onto pre-existing aerosols. Comparing AMS-sulfate (all sulfur species) to inorganic sulfate measured by online particle-into-liquid sampler−ion chromatography (PILS-IC), we find roughly 80% of sulfate increase was due to organic sulfur, consistent with the observation of mass spectral signatures in the AMS of organosulfur compounds. The rapid formation of sulfate appears to coincide with spikes in ambient aldehyde concentrations (formaldehyde and acetaldehyde) and an increase in S(IV) in ambient $PM_{2.5}$. This likely results from multiphase chemistry, where hydroxymethanesulfonate (HMS) and other aldehyde-S(IV) adducts are formed through reactions between aldehydes and SO_2 in deliquesced aerosols. We estimate that all S(IV) species, including HMS, contribute an average of 30% to aerosol sulfur, with a dominant fraction occurring during rapid sulfate increase events. Our work highlights the crucial role of controlling aldehydes to mitigate severe air pollution events in Fairbanks and may apply to other urban areas. It also emphasizes the significance of multiphase chemistry in driving particle growth from Aitken mode to accumulation mode, a key step for aerosol-cloud interactions.

1. Introduction

Sulfate comprises a significant portion of $PM_{2.5}$ mass in many urban winter environments. In Beijing (*1*) and Fairbanks (*2*), sulfate accounts for 10-20% of wintertime $PM_{2.5}$ mass, with even higher fractions observed during pollution events, reaching up to 50%. A large body of work has been devoted to understanding the mechanisms of SO_2 oxidation and sulfate formation (*3*–*5*), through oxidation occurring in both cloud droplets and deliquesced aerosols. However, the sulfate production in cloud droplets appears to be insufficient to explain the sulfate observed in urban environments (*6*). As a result, many sulfate pathways are proposed to take place in deliquesced aerosols, including oxidation by transition metal ions (*5*), NO_2 (*3*, *7*), H_2O_2 (*8*) and organic peroxides (*9*). However, all these studies are based on laboratory results and there have been no confirmation about what pathways actually dominate in various environment. One aspect is that these pathways are highly sensitive to aerosol acidity (*4*).

Fairbanks winter offers a unique opportunity to study sulfate formation, where the cold and dark conditions significantly limit photochemical activity. While a large fraction of sulfate originating from primary emissions, secondary formation may still contribute substantially to the sulfate mass (*10*). In addition, it was found that S(IV) species including hydroxymethanesulfonate (HMS) are particularly high in Fairbanks winter, accounting for 3-7% of $PM_{2.5}$ mass during pollution episodes, much higher than other studied urban areas (*11*, *12*). This is largely attributed to the indirect modulation of cold temperature on aerosol pH, promoting secondary formation in aerosols during severe pollution events (*13*).

Here we use the extensive measurements collected during the ALPACA 2022 field campaign and other winters, to better understand sulfate formation and particle growth in such cold and dark environments.

2. Measurements on aerosol composition and size distribution

During the ALPACA 2022 field campaign (Jan 15th-Feb 28th of 2022), we deployed two high-resolution time-of-flight aerosol mass spectrometers (HR-ToF-AMS) and one aerosol chemical speciation monitor (ACSM) at three urban sites (Figure 1), combined with two Scanning Mobility Particle Sizers (SMPS), to examine the evolution of aerosol composition and the size distribution at a sub-hourly time scale. The detailed site information is given in the overview paper (*14*). We will largely focus on the measurements at the CTC site and House site, with brief discussion on the measurements at the NCore site. As the CTC site is located in downtown Fairbanks and the House site is in a nearby residential area, roughly 3 km apart, we expect that the air masses at these two locations may be influenced by traffic and residential sources differently. Cloud processing is considered to be of minor importance in this work as there are few liquid clouds in Fairbanks winter (*15*).

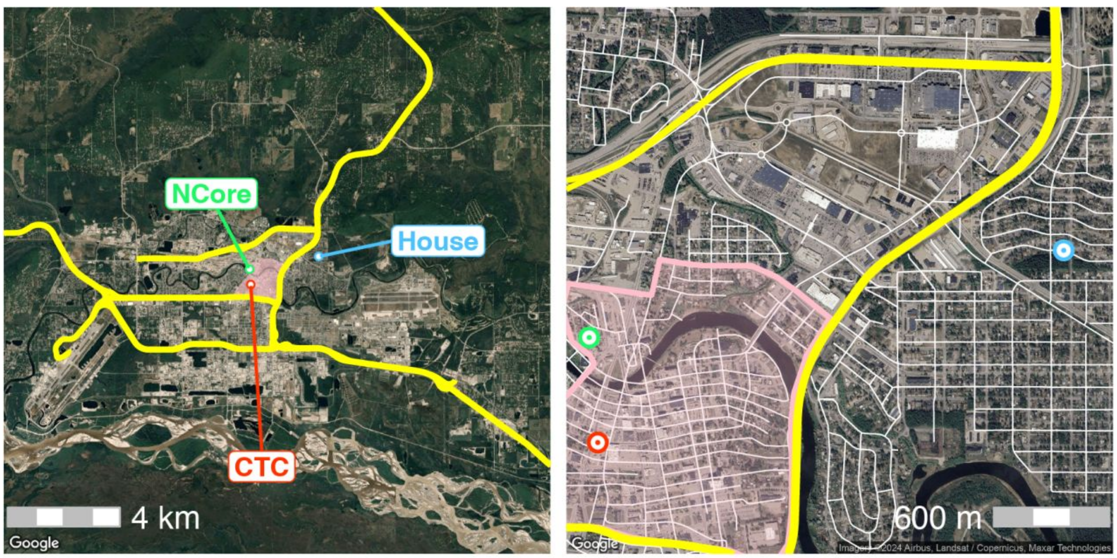

Figure 1: (Left) Map of the three sampling sites within the larger Fairbanks area. (Right) Zoomed-in map of the three sampling sites. Yellow lines highlight major highways and arterial roads, and the red polygon highlights the downtown area. Both the House and CTC sites were equipped with an HR-ToF-AMS and an SMPS, while the NCore site was equipped with an ACSM.

Both the House and CTC sites were equipped with an HR-ToF-AMS, while the NCore site was equipped with an ACSM. Both HR-ToF-AMS are equipped with a PM_1 aerodynamic lens and the standard vaporizer, while the ACSM is equipped with $PM_{2.5}$ aerodynamic lens and capture vaporizer. Both HR-ToF-AMS and ACSM measure organic, sulfate, nitrate, ammonium and chloride mass concentrations, at sub-hourly time resolution. Standard AMS data analysis assumes that all $H_xS_yO_z^+$ fragments are sulfate, though recent studies (*16*, *17*) show that subtle differences in $H_xS_yO_z^+$ fragmentation patterns has the potential to distinguish between sulfate and organosulfur compounds, such as HMS. For this analysis, we refer to all $H_xS_yO_z^+$ signal as “AMS-sulfate” following the standard convention. AMS-sulfate implicitly contains inorganic sulfate, organic sulfate, HMS and other S(IV) species, i.e. aerosol sulfur compounds. The HR-ToF-AMS at the

House site was operated in “particle time of flight (p-ToF)” mode (*18*), which provides particle mass size distributions for aerosol species and mass spectral fragments. In addition, the ACSM has been running at the NCore site from mid-January of 2020 to end of February of 2022. A detailed analysis on the ACSM dataset can be found in Robinson et al. (*2*)

Two Scanning Mobility Particle Sizer (SMPS) were deployed at both House site and CTC site, to measure the aerosol number size distribution from 15 nm to 660 nm at a time resolution of 1-3 min. The SMPS (model TSI 3936) deployed at the CTC site includes a 3080 Electrostatic Classifiers with a differential mobility analyzer (DMA 3081), a Condensation Particle Counter (CPC 3775), and a X-ray neutralizer 3087. The SMPS deployed at the House site was identical to the one at the CTC site with the exception of the CPC used for particle detection (CPC 3787). We emphasize that SMPS measures electrical mobility diameter (D_{mob}), which differs from the vacuum aerodynamic diameter (D_{va}) from p-ToF mode of HR-ToF-AMS. The two can be related through the density of particles (ρ_p) (*19*):

$$\frac{D_{va}}{D_{mob}} = \rho_p (1)$$

We include online particle-into-liquid sampler–ion chromatography (PILS-IC) measurements for aerosol S(IV) (*11*, *12*). Ambient formaldehyde (HCHO) measurements at the CTC site were made by a compact formaldehyde fluorescence experiment (COFFEE) instrument using a non-resonant laser induced fluorescence (NR-LIF) technique (St. Clair et al., 2017, 2019). Ambient HCHO at the House site was measured by Picarro G2307 gas analyzer using cavity ring-down spectroscopy (CRDS). Acetaldehyde (CH_3CHO) was measured by Proton Transfer Reaction – Mass Spectrometry (PTR-MS) at both sites. Total ammonium (NH_x, i.e. gas-phase NH_3 + aerosol ammonium NH_4^+) was measured at the CTC site by a mist chamber coupled to an cation IC (MC-IC) (*22*). Other measurements include temperature, wind, relative humidity (RH), O_3 (Thermo Scientific 49C), NO_x (Thermo Scientific 42C), and SO_2 (Thermo Scientific 43C) were available at CTC and NCore sites, and only a subset (temperature, wind, RH, O_3, NO_x) were available at the House site.

3. Results

We mainly focus on a cold pollution event encountered during ALPACA 2022 field campaign. This event spanned from Jan 29th to the early afternoon of Feb 3rd, with temperature between -20 and -35 °C and calm conditions (wind speed < 1 m/s) for most of the time. The pollution event concluded on February 3rd due to a snowfall. A strong surface-based inversion layer was present throughout this event, leading to heavy pollution with hourly $PM_{2.5}$ over 80 μg/m³ (*14*). In Figure 2, we show that during this period ambient NO_x levels are between 100 and 200 ppbv in downtown Fairbanks, leading to full titration of O_3 and likely very low oxidant levels. Ambient SO_2 concentrations varied between 15 and 40 ppbv, to a large extent driven by heating oil combustion. The campaign average in downtown Fairbanks shows a $PM_{2.5}$ mass concentration of 12 μg/m³, with SO_2 levels at 10 ppb and NO_x concentrations at 65 ppb. A number of studies have examined different aspects in Fairbanks wintertime air pollution, including aerosol pH (*13*), oxidative potential (*23*), aerosol sulfur speciation (*12*), sulfur emissions (*10*) and NO_x emissions (*24*).

3.1 Multiphase sulfur chemistry (CTC site)

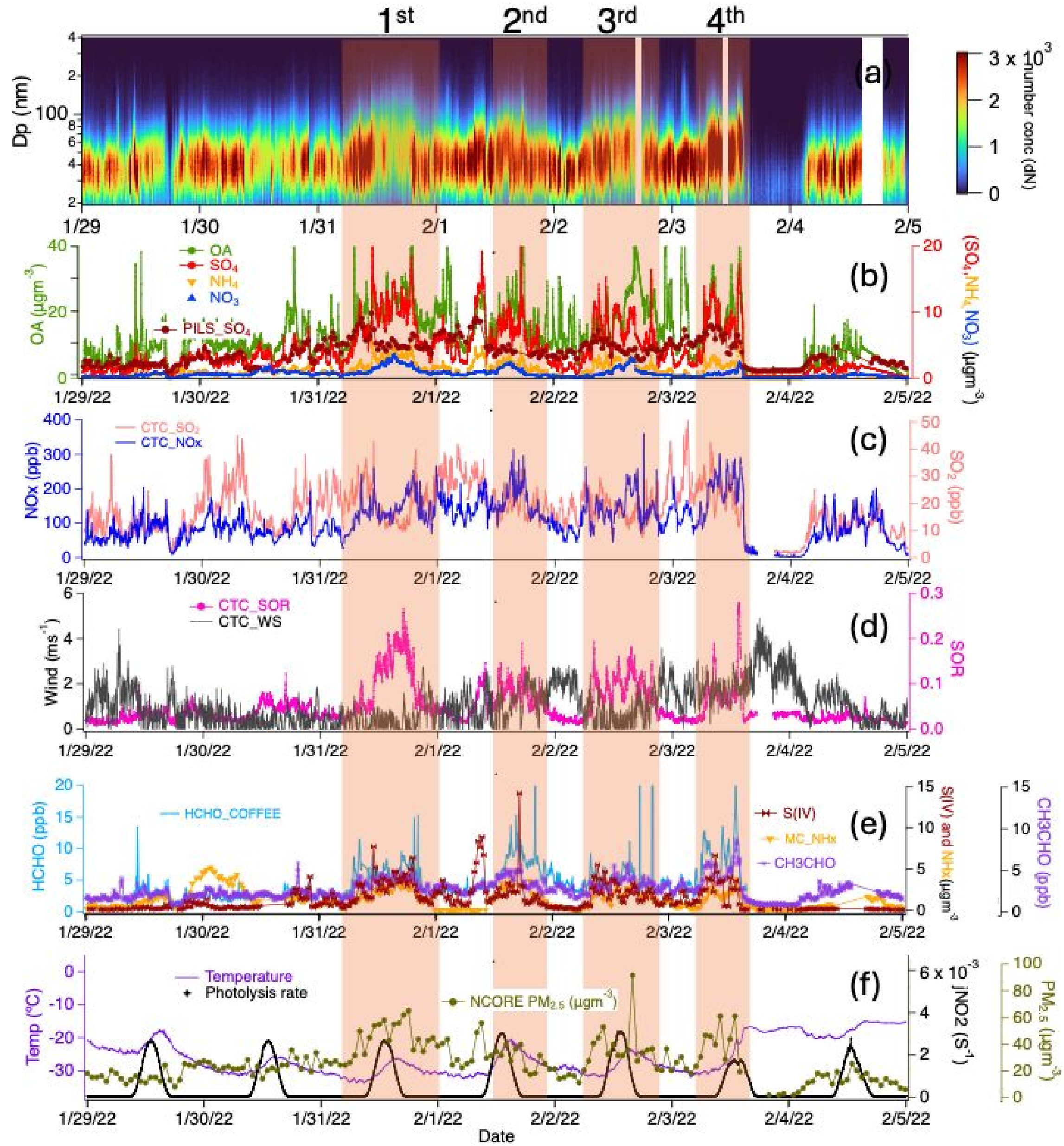

Figure 2. Measurements at the CTC site during the severe pollution episode from Jan 29th to Feb 3rd of 2022. Panel (a) shows aerosol number size distribution measured by SMPS; Panel (b) shows PM_1 OA, sulfate, nitrate and ammonium mass concentrations from HR-ToF-AMS and $PM_{2.5}$ sulfate from PILS-IC; Panel (c) shows the measured SO_2 and NO_x volume mixing ratio; Panel (d) shows the wind speed and calculated sulfate oxidation ratio (SOR) based on measured gaseous SO_2 and AMS-sulfate concentrations; Panel (e) shows the measured HCHO volume mixing ratio from COFFEE, CH_3CHO volume mixing ratio from PTR-MS, S(IV) concentrations from PILS-IC and total ammonium (NH_x) from Mist Chamber-IC; Panel (f) shows the ambient temperature, hourly $PM_{2.5}$ mass measured by Beta Attenuation Mass Monitor (Met One BAM 1020) and NO_2 photolysis rates (j_{NO2}) measured by Diode-array Actinic Flux Spectroradiometer ($PM_{2.5}$ mass and j_{NO2} measured at NCore site).

The measurements at CTC site provided a detailed examination at multiphase chemistry during this cold event. Despite high levels of SO_2 and NO_2, AMS-sulfate mass remained low on Jan 29th and 30th, below 3 μg/m³ (Figure 2b). There were cold and calm conditions with temperatures less than -30 ℃ and wind speeds less than 1 m/s. Ambient NO_x levels were relatively stable near 100 ppbv, while SO_2 exhibited significant temporal variability, ranging from 10 to 40 ppbv. This difference in temporal variability between SO_2 and NO_x may reflect the mixing of different air masses from heating oil combustion and vehicle exhaust at a neighborhood level, as heating oil combustion is rich in both SO_2 and NO_x emissions and vehicle exhaust is only rich in NO_x emissions (*24*). This mixing may be partly driven by the buoyancy of household heating oil exhaust plumes, which are emitted hot and with abundant moisture. Since neighborhood chimneys are typically 5 meters or less in height, the exhaust plumes remain within the surface-based inversion (SBI) and may lead to some local mixing. In fact, SO_2 reached its maximum every early morning from Jan 30th to Feb 3rd while NO_x did not, further supporting that SO_2 and NO_x have different source profiles. We further note that while SO_2 spiked up to 40 ppbv in the early morning of Jan 30th, there was little corresponding increase in AMS-sulfate, and HCHO levels were around 2-4 ppb during this time, suggesting heating oil combustion may not be a major source of HCHO in downtown Fairbanks. We calculated sulfate oxidation ratio (SOR), which was around 5%, in agreement with estimated primary sulfate emissions (*25*).

AMS-sulfate spikes did not appear until the third day of this cold event, Jan 31st. These sulfate spikes show very high level of AMS-sulfate (10-20 μg/m³) under very calm conditions (wind speed < 1 m/s) and can last for a few hours. Both aerosol nitrate and ammonium show simultaneous increases, suggesting an internal mixture of these inorganic components and potentially deliquesced aerosols. Organic mass also shows increases coinciding with these AMS-sulfate spikes. Combining ambient SO_2 measurements and AMS-sulfate, SOR increases from 5% to 10-20% during these sulfate spikes. Figure 2b and 2c show that ambient SO_2 significantly dropped during the sulfate spikes on Jan 31st, Feb 1st and 2nd. The simultaneous rise in ambient AMS-sulfate mass and decline in SO_2 concentrations is consistent with the conversion of SO_2 to a different form in ambient air, suggesting secondary formation of aerosol sulfur.

The AMS-sulfate spikes are strongly related to the simultaneous increases of formaldehyde (HCHO), acetaldehyde (CH_3CHO) and S(IV) levels (Figure 2e). We show that while HCHO remained at 2-4 ppbv in the first two days it increased to 6-10 ppbv on Jan 31st. CH_3CHO shows a similar behavior. While the sources of these aldehydes are still unclear, the enhancement of HCHO, CH_3CHO and S(IV) appears to coincide with AMS-sulfate spikes, potentially through the formation of HMS and other aldehyde-adducts (*11*, *12*). This suggests that aldehydes play a role in the rapid sulfate increases through the formation of HMS and other S(IV) species.

We further examine the aerosol sulfur speciation by comparing AMS-sulfate, PILS-sulfate and PILS-S(IV) (Figure 2b and e). As shown in Figure 2b, we find very little enhancement of PILS-sulfate during the AMS-sulfate spikes. Assuming the AMS-sulfate contains all aerosol sulfur compounds and PILS-sulfate only contains inorganic sulfate, this would suggest that the majority of AMS-sulfate enhancement is not due to inorganic sulfate. In fact, the AMS-sulfate spikes are mostly driven by the enhancement of S(IV) species. For the spike on Jan 31st, AMS-sulfate increases as much as 10 μg/m³, while the S(IV) enhancement is roughly 8 μg/m³, among which 50-60% is HMS (*12*). The rest of S(IV) is not well constrained, but one possibility is the formation of hydroxyethanesulfonate (HES), a CH_3CHO-S(IV) adduct similar as HMS (*26*, *12*). This is further supported by a Positive Matrix Factorization (PMF) analysis of combined organic and inorganic HR-ToF-AMS mass spectra, highlighting the role of organosulfur compounds for sulfate spikes (Ijaz et al., in prep). Throughout the cold event, PILS-S(IV) accounts for 30% of AMS-sulfate, with a dominant fraction occurring during rapid sulfate increase events.

Another prominent feature is the particle size shift during the sulfate spikes. Figure 2a shows that sulfate spikes are accompanied by shift in particle sizes. During the first and third sulfate spikes, the majority of 40 nm particles grow into larger sizes, with little change in the total number concentrations, suggesting particle growth on existing particles. The significant growth of particle sizes coincides with the enhancement in HCHO and HMS, suggesting the role of multiphase chemistry being responsible for particle growth. We further calculate the relative change of aerosol mass based on SMPS number size distribution, and they are consistent with the HR-ToF-AMS measurements (Figure S1). This confirms the role of multiphase sulfur chemistry in facilitating particle growth from the Aitken mode to the accumulation mode.

3.2 Particle growth due to increased sulfate mass (House site)

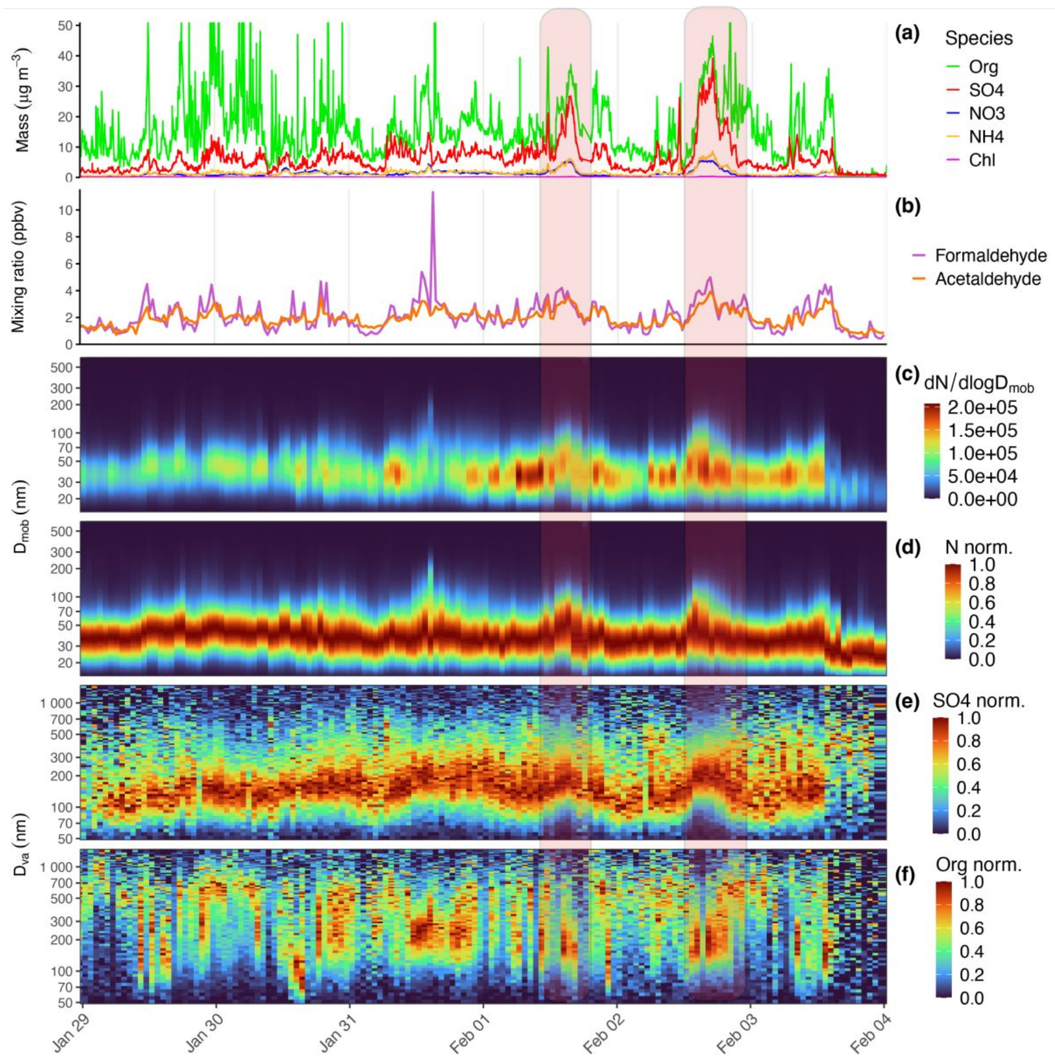

Figure 3. (a) Time series of PM_1 mass concentrations (μg/m³) from HR-ToF-AMS at the House site during the cold event period. (b) Ambient gas-phase formaldehyde (HCHO) and acetaldehyde (CH_3CHO) concentrations measured by Picarro and PTR-MS respectively. (c) Aerosol number size distribution $dN/dlogD_{mob}$ measured by SMPS. (d) Aerosol number size distribution normalized by the maximum value in this distribution. (e) Size-resolved sulfate mass measured by p-ToF HR-ToF-AMS. (f) Size-resolved organic mass measured by p-ToF HR-ToF-AMS.

We now examine the same pollution event at the House site, which is about 3 km away from the CTC site and located in a residential area (Figure 1). While there was no in-situ aerosol S(IV) or SO_2 measurements at this site, the HR-ToF-AMS instrument was operated at p-ToF mode, providing size-resolved aerosol composition. Figure 3a shows that on Jan 30th, while OA spikes reached as much as 50 μg/m^3, AMS-sulfate remains below 5 μg/m³. Similar to the CTC site, the AMS-sulfate spikes did not start until the third day (Jan 31st). In particular, the sulfate peak values reached 30-40 μg/m^3 on Feb 1st and 2nd, accounting for nearly half of the $PM_{2.5}$ mass increase for this highly polluted episode. The relative increase of AMS-sulfate at the House site is higher than that at the CTC site by a factor of 2-3 (Figures 3a and 2b). Such large spatial variability of aerosol mass concentrations is consistent with mobile sampling during the same period (*27*). Similar to the CTC site, the rapid increase in sulfate is accompanied by elevated gas-phase HCHO and CH_3CHO (Figure 3b), highlighting a similar multiphase sulfur chemistry at both sites.

Besides the rapid increase of aerosol mass, we show in Figure 3c and 3d that the particle number size distribution from SMPS has shifted significantly during rapid increase of sulfate mass. On both Feb 1st and Feb 2nd, aerosol sizes have shifted from the peak number concentration at 35 nm to 80 nm, suggesting particle growth of these Aitken mode particles.

We further illustrate this evolution in detail for the afternoon of Feb 2nd. Figure 4a and b show the time evolution of aerosol size distribution in both number and volume. At 1200h of Feb 2nd, the particle number concentration $dN/dlogD_{mob}$ peaks at 35 nm. In next few hours, the number distribution steadily shifts towards larger size bins, leading to $dN/dlogD_{mob}$ peaking at 60 nm at 1400h, roughly at a growth rate of 15 nm/h. We note that the total number concentrations remain roughly constant from 1200h to 1500h, suggesting that the gain of aerosol mass is related to aerosol growth on pre-existing particles, rather than from primary emissions. The shift of number size distribution towards smaller sizes at 1500h is likely due to the replenishment of primary emissions of ultrafine particles (<40 nm). After 1600h, a decrease in sulfate mass and organic mass is observed, likely due to mixing with air masses with low sulfate. This is consistent with the OA spikes measured by p-ToF measurements, which shows organic mass is mainly in the size range of 600-900 nm (Figure 3f).

This evolution of aerosol size growth leads to the rapid increase in aerosol mass, supported by the evolution of aerosol volume size distribution, $dV/dlogD_{mob}$. At 1200h of Feb 2nd, the aerosol volume was broadly distributed between 40 nm and 300 nm. Afterward, the total volume steadily increased, with the peak size shifting from 50 nm to 120 nm at 1400h. From 1400h to 1600h, the volume distribution remained relatively constant, indicating that the observed changes in number concentration were primarily due to an increase in Aitken mode particles that carry little mass.

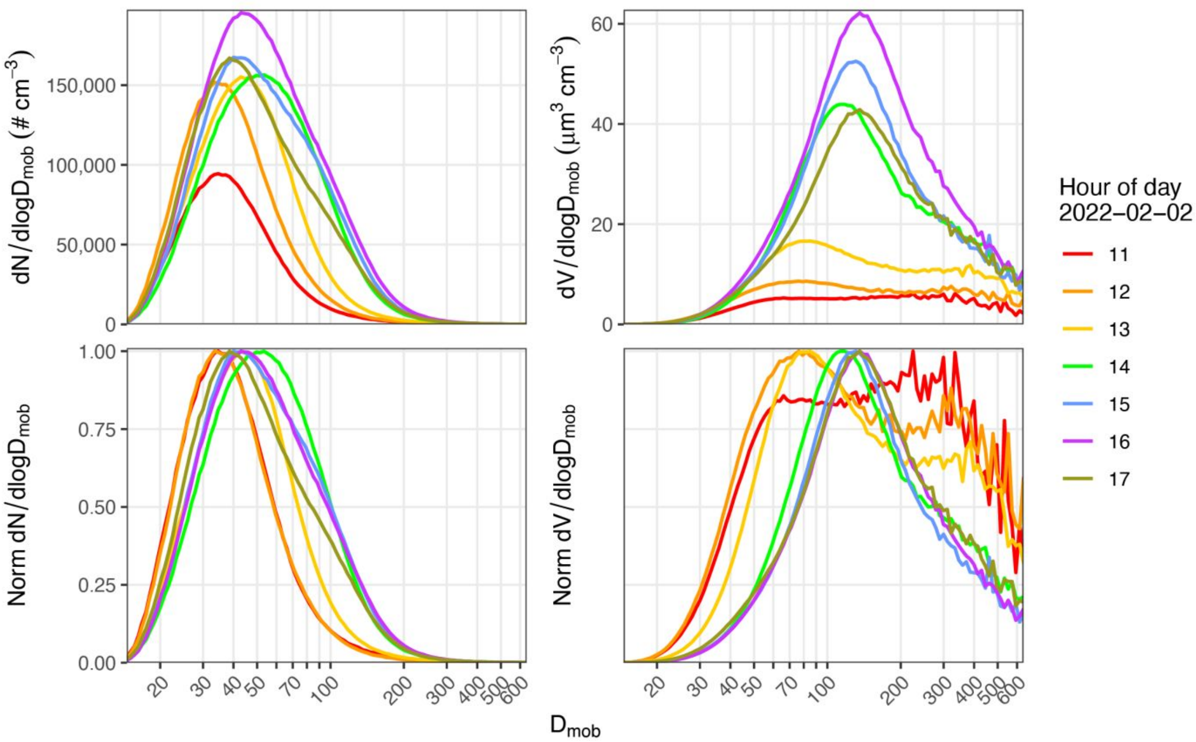

Figure 4. Time evolution of (a) aerosol number size distribution and (b) volume size distribution for the rapid increase of sulfate from 1100h to 1700h on Feb 2[nd] of 2022. The normalized distribution for the number size distribution and volume size distribution are shown in (c) and (d) respectively.

The aerosol growth recorded by the SMPS is consistent with the size-resolved aerosol composition measured by the HR-ToF-MS in p-ToF mode. Figure 3e shows that on Feb 2[nd], the sulfate mass distribution, measured by HR-ToF-MS, is primarily concentrated in the vacuum aerodynamic diameter (D_{va}) range of 70–150 nm prior to the rapid increase. Assuming particle density of 1.5 g/cm^3, this will translate into an electrical mobility diameter (D_{mob}) of 40-100 nm (Eq. (1)), consistent with the number distribution measured by SMPS (Figure 3c). Following the rapid increase in sulfate, the mass loading shifts towards larger particles, concentrating in the D_{va} size range of 120–250 nm, corresponding to a D_{mob} size range of 80–160 nm in the SMPS measurement. The concurrence of aerosol growth and the increase in sulfate mass within the same size ranges suggests that the growth event is driven in part by the rise in sulfate mass, along with a simultaneous increase in organic mass. This is further confirmed by the good agreement between SMPS-derived aerosol mass concentrations and AMS measured mass concentrations (Figure S2).

3.3 Ubiquity of rapid sulfate increase in Fairbanks winter

We further examined the ACSM measurements across three winters from 2020 to 2022. Unlike AMS, ACSM measurements have a time resolution of approximately 30 min. As ACSM was located at the NCore site, we were able to include co-located NO_y and SO_2 measurements provided by Alaska Department of Environmental Conservation (ADEC) in this analysis. We illustrate a number of additional sulfate spiking events observed in the ACSM dataset in the SI throughout these winters (Figures S3, S4 and S5). Similar to the cold event shown in Figures 2 and 3, these rapid sulfate increase events tend to last a few hours. This is in contrast to the steady, days-long increases of sulfate found in winter haze in China (*28*). Another feature is the relative enhancement of AMS-sulfate during periods of high PM event. We find that the hourly SO_4/OA mass ratio ranges roughly from 0.3 to 1.0 during these high PM events, suggesting OA might play a role in the sulfate growth event.

We summarize the ACSM results from 2020 to 2022 in Figure 5. We further define sulfate spiking events as hourly averaged $SO_4/OA > 0.35$ and $PM_{2.5} > 30$ µg/m³. Between November and February across 2020-2022, we recorded a total of 256 ACSM measurement days, 39 of which (15%) experienced sulfate spiking events. Figure 5 clearly shows that sulfate spiking events occurred during periods of high NO_y, SO_2, and CO, combined with low ambient temperatures—conditions that favor strong surface inversions and poor air quality. This is consistent with the cold event presented above. One key feature is that sulfate spiking events are present in high $PM_{2.5}$ events, highlighting the critical role of aerosol sulfur in exacerbating air pollution (*2*). It also appears that sulfate spiking events do not take place when ambient temperature is higher than -15℃, a condition that is most common in mid-latitude urban winters (*13*).

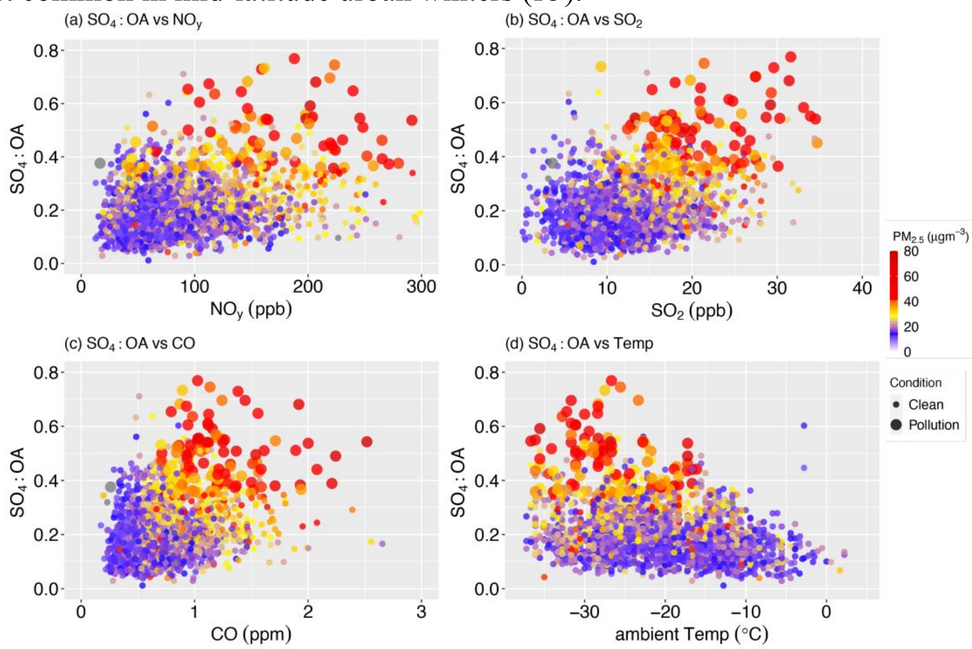

Figure 5 Correlation plot between SO_4/OA mass ratio from ACSM in three winters and (a) NO_y concentrations, (b) SO_2 concentrations, (c) CO concentrations and (d) ambient temperature from ADEC. We only use the data from Nov to Feb in 2020-2022. Each dot represents an hourly-averaged measurement and is color-coded based on hourly $PM_{2.5}$ data from the BAM at ADEC. Larger dots represent $PM_{2.5} > 30$ µg/m³ as indicated as pollution, while smaller dots represent $PM_{2.5} < 30$ µg/m³ as indicated as clean.

3.4 A link between multiphase sulfur chemistry and particle growth

Growth of Aitken mode particles (>25 nm in diameter) in urban areas is often a result of condensational growth, as coagulation is too slow to be important (*29*). Condensational growth can occur by either condensation of low volatile species formed in the gas phase (e.g., SO_2 (g) + OH (g) → H_2SO_4 (g) → SO_4^{2-} (aq)), or by formation of low volatile species in the particle phase (e.g., SO_2 (g) → SO_2 (aq) → aerosol sulfur compounds). In Fairbanks winter, the growth of Aitken mode particles is unlikely driven by the condensation of inorganic or low-volatility organic species. This is because sulfuric acid vapor and highly oxygenated organic molecules (HOMs) are expected to be low during the Fairbanks winter, given the limited sunlight and extremely low photochemical activity (i.e., low O_3 and gas-phase OH concentrations). The only plausible explanation is multiphase chemistry through aerosol surfaces. We also emphasize that the rapid increase of sulfate in a short timescale is also a sign of surface-area-driven process, rather than partitioning-driven process (*30*).

One potential pathway for particle growth is through the production of hydroxymethanesulfonate (HMS) and other S(IV) species in the Aitken mode aqueous particles. The detailed mechanism of HMS and other S(IV) formation can be found elsewhere (*11*, *12*). We emphasize that HMS and other S(IV) formation is substantially favored at low temperature, both directly through enhanced solubility and indirectly through modulation of aerosol pH (*13*).

Mass spectral changes measured by the AMS are consistent with the formation of organosulfur compounds during these growth events. Figure 6 shows three spectra for $H_xS_yO_z^+$ fragments, including a four-hour-long average spectra during the Feb. 2 growth event, a day-long average spectra during a day (Feb. 18) where no such growth events were observed and the ammonium sulfate likely dominates the AMS-sulfate (compared to organosulfur compounds), and pure ammonium sulfate from calibration. The growth event spectra show signatures that are consistent with spectra from laboratory studies on organosulfur standards in Chen et al. (*16*) and Dovrou et al. (*17*), and different from pure ammonium sulfate, namely low HSO_3^+/SO^+ and $H_2SO_4^+/SO^+$ and high SO_2^+/SO^+ ratios. Similar changes in the fragmentation pattern of AMS-sulfate were observed by the ACSM at the NCore site, showing a dependence on total $PM_{2.5}$ concentration. As reported by Robinson et al. (*2*), periods of high $PM_{2.5}$ concentrations were characterized by decreased HSO_3^+/SO^+ and $H_2SO_4^+/SO^+$ ratios.

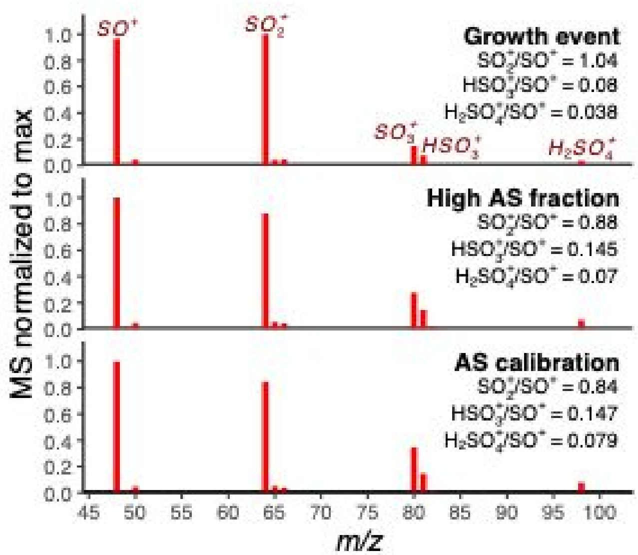

Figure 6. HR-ToF-AMS spectra of $H_yS_xO_z^+$ fragments collected at the House site for three cases: (a) a four-hour-long average spectra during the Feb. 2 growth event, (b) a day with no observed growth events (Feb. 18), where AMS-sulfate concentrations were low, and (c) pure ammonium sulfate from calibrations. Ratios of major $H_yS_xO_z^+$ fragments relative to SO^+ are shown in each panel.

In contrast to previous studies on sulfate formation in the presence of NO_2 (*3*, *7*), we do not find that SO_2 oxidation by NO_2 pathway is effective in rapid production of sulfate. First, Figure 6 shows the mass spectra of AMS-sulfate fragments during the growth event are not consistent with ammonium sulfate, but are consistent with the presence of organosulfur compounds, such as HMS and potentially other aldehyde-S(IV) adducts, as demonstrated by measurements of laboratory organosulfur standards (Chen et al., 2021; Dovrou et al., 2019). Second, despite high levels of SO_2, NO_x and NH_x on Jan 30th (Figure 3), we do not see rapid increase of AMS-sulfate. While SO_2, NO_x and NH_x remained high on Jan 31st, we start to see the AMS-sulfate spikes coincident with HCHO enhancements. We consider the role of transition metal ions (TMI) on sulfate formation to be unimportant, as single particle measurements find that most sulfate-containing particles do not contain transition metals (Kerri Pratt, personal communication). The oxidation of SO_2 by H_2O_2 is independent of aerosol pH and potentially slow (*8*). These suggest that the rapid sulfate increase is most likely triggered by HCHO or species co-emitted with HCHO and is observed at both the CTC and House sites. We emphasize that these pathways involving TMI, H_2O_2, and NO_2 may contribute more significantly over extended periods in background air masses, as suggested by filter analysis (*10*).

If HCHO and other aldehydes trigger aerosol sulfur formation and particle growth, the process may occur as follows. The process starts with many small primary sulfate-containing particles (30-50 nm) mainly from heating oil combustion, mixed with high level of gaseous NO_x, SO_2 and NH_3 from vehicle emissions and other sources. At this time, the majority of organic aerosol mass reside in the large size bins (>500 nm) (Figure 3f). pH of these small sulfate-containing particles is 4-5 (*13*). Once HCHO emissions increase, small sulfate-containing particles, which carry the majority of aerosol surface area, provide aqueous surfaces on super-cooled droplets for both SO_2 and HCHO partitioning into the particle phase, leading to the formation of HMS and other aldehyde-adducts. As both HMS and other aldehyde-adducts are highly hygroscopic, the formation of these S(IV) species leads to increase of both aerosol sulfate mass and aerosol liquid water, as well as ammonium and nitrate in the aerosol phase. At these low temperatures, NH_3 partitioning into the particle phase is strongly favored, and aerosol pH ranges from 4 to 5 when total NH_x is in excess (*13*). This promotes the self-accelerating formation of HMS and other S(IV) species due to the increased surface area, resulting in a rapid rise in detected AMS-sulfate. Note that HMS is a strong acid with $pK_a < 0$ (*11*). Once the concentration of HMS and other aldehyde-adducts becomes sufficient relative to total NH_x (when the total Ammonium to total Sulfate molar ratio drops below 2) in individual particles, HMS formation will cease because of the resulting large drop in aerosol pH (*13*). Potentially the relative increase of sulfate depends on the supply of ambient NH_3. This would also explain the sulfate enhancements only lasting for a few hours (Figures 2, 3 and 5). The particle growth event ends with mixing with air masses low in sulfate but potentially high in SO_2 or OA (Jan 31st, Feb 1st in Figure 3) or just increased wind speed and precipitation (Feb 2nd and 3rd in Figure 2).

4. Implications

Sulfate accounts for an average of 20% of $PM_{2.5}$ mass during Fairbanks winters (*2*). A substantial portion of the aerosol sulfate comes from primary emissions, such as residential heating oil combustion (*10*). These primary emissions comprise small sulfate particles in the Aitken mode (Figure 2), often less than 50 nm in diameter. Growth from Aitken mode into accumulation mode is a critical step to understand aerosol-cloud interaction, contributions of particles to direct radiative effects, and the increase in $PM_{2.5}$ mass concentration, but the mechanism remains to be elucidated.

Here we show the direct observation of particle growth from Aitken mode (0.01 to 0.1 μm diameter) into the accumulation mode (0.1 to 1 μm diameter), during strong inversion conditions in Fairbanks winter. We show that this growth of sulfate only lasts for a few hours but can produce as much as 30-40 μg/m³ AMS-sulfate, accounting for nearly half of $PM_{2.5}$ during severe pollution events. The sulfate growth is often accompanied by rapid increases of OA, nitrate and ammonium. We find that these particle growth events are likely driven by multiphase chemistry, triggered by emissions of formaldehyde and other aldehydes, where HCHO is most important as HMS accounts for the majority of aerosol S(IV) (*12*). Our results suggest that the SO_2 oxidation by NO_2 pathway alone does not appear to be effective in converting SO_2 to sulfate, despite high concentrations of SO_2 and NO_2, enhanced solubility driven by low temperatures and favorable pH conditions. Instead, the observed rapid increase of AMS-sulfate mass is initiated once the HCHO ambient level is enhanced, indicating a role of HCHO in driving the aerosol chemistry. This is somewhat different from a recent study on the catalytic role of HCHO on in-cloud processing (*31*), as liquid cloud droplets are absent in Fairbanks winter (*15*). The relative increase of aerosol sulfur appears to be dependent on the amount of NH_3 supply as the growth would cease when aerosol becomes acidic.

This work can provide insights and constraints on the formation pathways of sulfate aerosol in cold urban areas (e.g. winter haze in China). While many studies have speculated the role of NO_2 on SO_2 oxidation (*3*, *4*), we find that only NO_2 and SO_2 in a cold and dark environment with pre-existing particles are inadequate to convert SO_2 to sulfate aerosol. The sulfate formation in aerosols, however, can be largely facilitated by the addition of HCHO to the environment, similar to its role in the cloud-processing of SO_2 as noted by others (*32*). Although rapid sulfate formation in aerosols only lasts for a few hours, it can produce substantial amounts of aerosol sulfur and potentially other species, significantly worsening air quality during pollution events. Our work has important implications on controlling severe pollution events in cold and dark environments.

Acknowledgement
J.M., J.R.C. and K.B. were supported by the National Science Foundation (NSF) Atmospheric Geoscience Program (grant no. AGS-2029747) and the NSF Navigating the New Arctic Program (grant no. NNA-1927750). R.J.W. was supported by the NSF Atmospheric Geoscience Program (grant no. AGS-2029730) and the NSF Navigating the New Arctic Program (grant no. NNA-1927778). F.G. and J.H.F. were supported by the NSF Atmospheric Geoscience Program (grant no. AGS-2109098). J.M.S.C. acknowledges support from the NASA Tropospheric Composition Program and the NSF Atmospheric Chemistry Program (grant no. 2029770).

A.I., B.D and B.T-R were supported by the CASPA (Climate-relevant Aerosol Sources and Processes in the Arctic) project of the Agence Nationale de la Recherche (grant no. ANR-21-CE01-0017) and INSU-CNRS (National Institute of Sciences of the Universe) via its national LEFE program and IPEV (French Polar Institute Paul-Émile Victor).

Funding support for E. S. R. and P. F. D. comes from the U.S. National Science Foundation's (NSF) Navigating the New Arctic (NNA) Program (grant nos. NNA-90086753 and NNA-1927750).

W.R.S. and M.C.-M. acknowledge support from NSF grant AGS-2109134 and NNA-1927750.

L. H. and R. Y. were supported by NOAA Climate Program Office's Atmospheric Chemistry, Carbon Cycle, and Climate program, grant number NA20OAR4310296.

Author contribution:
Conceptualization: J.M., Methodology: J.M., K.B., E.S.R., R.J.W., Investigation: J.M., K.B., E.S.R., R.J.W., R.J.K., Visualization: J.M., K. B., E.S.R., Writing—original draft: J.M., E.S.R., R.J.W., with edits from all coauthors.

References

1. G. Wang, R. Zhang, M. E. Gomez, L. Yang, M. Levy Zamora, M. Hu, Y. Lin, J. Peng, S. Guo, J. Meng, J. Li, C. Cheng, T. Hu, Y. Ren, Y. Wang, J. Gao, J. Cao, Z. An, W. Zhou, G. Li, J. Wang, P. Tian, W. Marrero-Ortiz, J. Secrest, Z. Du, J. Zheng, D. Shang, L. Zeng, M. Shao, W. Wang, Y. Huang, Y. Wang, Y. Zhu, Y. Li, J. Hu, B. Pan, L. Cai, Y. Cheng, Y. Ji, F. Zhang, D. Rosenfeld, P. S. Liss, R. A. Duce, C. E. Kolb, M. J. Molina, Persistent sulfate formation from London Fog to Chinese haze. *Proc. Natl. Acad. Sci.* **113**, 13630–13635 (2016).

2. E. S. Robinson, J. Michael Battaglia, J. R. Campbell, M. Cesler-Maloney, W. Simpson, J. Mao, R. J. Weber, P. F. DeCarlo, Multi-year, high-time resolution aerosol chemical composition and mass measurements from Fairbanks, Alaska. *Environ. Sci. Atmospheres*, doi: 10.1039/D4EA00008K (2024).

3. Y. Cheng, G. Zheng, C. Wei, Q. Mu, B. Zheng, Z. Wang, M. Gao, Q. Zhang, K. He, G. Carmichael, U. Pöschl, H. Su, Reactive nitrogen chemistry in aerosol water as a source of sulfate during haze events in China. *Sci. Adv.* **2** (2016).

4. T. Liu, A. W. H. Chan, J. P. D. Abbatt, Multiphase Oxidation of Sulfur Dioxide in Aerosol Particles: Implications for Sulfate Formation in Polluted Environments. *Environ. Sci. Technol.* **55**, 4227–4242 (2021).

5. W. Wang, M. Liu, T. Wang, Y. Song, L. Zhou, J. Cao, J. Hu, G. Tang, Z. Chen, Z. Li, Z. Xu, C. Peng, C. Lian, Y. Chen, Y. Pan, Y. Zhang, Y. Sun, W. Li, T. Zhu, H. Tian, M. Ge, Sulfate formation is dominated by manganese-catalyzed oxidation of SO2 on aerosol surfaces during haze events. *Nat. Commun.* **12**, 1993 (2021).

6. T. Wang, M. Liu, M. Liu, Y. Song, Z. Xu, F. Shang, X. Huang, W. Liao, W. Wang, M. Ge, J. Cao, J. Hu, G. Tang, Y. Pan, M. Hu, T. Zhu, Sulfate Formation Apportionment during Winter Haze Events in North China. *Environ. Sci. Technol.* **56**, 7771–7778 (2022).

7. T. Liu, J. P. D. Abbatt, Oxidation of sulfur dioxide by nitrogen dioxide accelerated at the interface of deliquesced aerosol particles. *Nat. Chem.*, 1–5 (2021).

8. T. Liu, S. L. Clegg, J. P. D. Abbatt, Fast oxidation of sulfur dioxide by hydrogen peroxide in deliquesced aerosol particles. *Proc. Natl. Acad. Sci.* **117**, 1354–1359 (2020).

9. S. Wang, Y. Zhao, A. W. H. Chan, M. Yao, Z. Chen, J. P. D. Abbatt, Organic Peroxides in Aerosol: Key Reactive Intermediates for Multiphase Processes in the Atmosphere. *Chem. Rev.* **123**, 1635–1679 (2023).

10. A. Moon, U. Jongebloed, K. K. Dingilian, A. J. Schauer, Y.-C. Chan, M. Cesler-Maloney, W. R. Simpson, R. J. Weber, L. Tsiang, F. Yazbeck, S. Zhai, A. Wedum, A. J. Turner, S. Albertin, S. Bekki, J. Savarino, K. Gribanov, K. A. Pratt, E. J. Costa, C. Anastasio, M. O. Sunday, L. M. D. Heinlein, J. Mao, B. Alexander, Primary Sulfate Is the Dominant Source of Particulate Sulfate during Winter in Fairbanks, Alaska. *ACS EST Air*, doi: 10.1021/acsestair.3c00023 (2023).

11. J. R. Campbell, M. Battaglia, K. Dingilian, M. Cesler-Maloney, J. M. St Clair, T. F. Hanisco, E. Robinson, P. DeCarlo, W. Simpson, A. Nenes, R. J. Weber, J. Mao, Source and Chemistry of Hydroxymethanesulfonate (HMS) in Fairbanks, Alaska. *Environ. Sci. Technol.*, doi: 10.1021/acs.est.2c00410 (2022).

12. K. Dingilian, E. Hebert, M. Jr. Battaglia, J. R. Campbell, M. Cesler-Maloney, W. Simpson, J. M. St. Clair, J. Dibb, B. Temime-Roussel, B. D’Anna, A. Moon, B. Alexander, Y. Yang, A. Nenes, J. Mao, R. J. Weber, Hydroxymethanesulfonate and Sulfur(IV) in Fairbanks Winter During the ALPACA Study. *ACS EST Air*, doi: 10.1021/acsestair.4c00012 (2024).

13. J. R. Campbell, Michael, K. K. Dingilian, M. Cesler-Maloney, W. R. Simpson, E. S. Robinson, P. F. DeCarlo, B. Temime-Roussel, B. D’Anna, A. L. Holen, J. Wu, K. A. Pratt, J. E. Dibb, A. Nenes, R. J. Weber, J. Mao, Enhanced aqueous formation and neutralization of fine atmospheric particles driven by extreme cold. *Sci. Adv.* **10**, eado4373 (2024).

14. W. R. Simpson, J. Mao, G. J. Fochesatto, K. S. Law, P. F. DeCarlo, J. Schmale, K. A. Pratt, S. R. Arnold, J. Stutz, J. E. Dibb, J. M. Creamean, R. J. Weber, B. J. Williams, B. Alexander, L. Hu, R. J. Yokelson, M. Shiraiwa, S. Decesari, C. Anastasio, B. D’Anna, R. C. Gilliam, A. Nenes, J. M. St. Clair, B. Trost, J. H. Flynn, J. Savarino, L. D. Conner, N. Kettle, K. M. Heeringa, S. Albertin, A. Baccarini, B. Barret, M. A. Battaglia, S. Bekki, T. J. Brado, N. Brett, D. Brus, J. R. Campbell, M. Cesler-Maloney, S. Cooperdock, K. Cysneiros de Carvalho, H. Delbarre, P. J. DeMott, C. J. S. Dennehy, E. Dieudonné, K. K. Dingilian, A. Donateo, K. M. Doulgeris, K. C. Edwards, K. Fahey, T. Fang, F. Guo, L. M. D. Heinlein, A. L. Holen, D. Huff, A. Ijaz, S. Johnson, S. Kapur, D. T. Ketcherside, E. Levin, E. Lill, A. R. Moon, T. Onishi, G. Pappaccogli, R. Perkins, R. Pohorsky, J.-C. Raut, F. Ravetta, T. Roberts, E. S. Robinson, F. Scoto, V. Selimovic, M. O. Sunday, B. Temime-Roussel, X. Tian, J. Wu, Y. Yang, Overview of the Alaskan Layered Pollution and Chemical Analysis (ALPACA) Field Experiment. *ACS EST Air*, doi: 10.1021/acsestair.3c00076 (2024).

15. C. G. Schmitt, D. Vas, M. Schnaiter, E. Järvinen, L. Hartl, T. Wong, V. Cassella, M. Stuefer, Microphysical characterization of boundary layer ice particles: results from a 3-year measurement campaign in interior Alaska. *J. Appl. Meteorol. Climatol.* **1** (2024).

16. Y. Chen, L. Xu, T. Humphry, A. P. S. Hettiyadura, J. Ovadnevaite, S. Huang, L. Poulain, J. C. Schroder, P. Campuzano-Jost, J. L. Jimenez, H. Herrmann, C. O’Dowd, E. A. Stone, N.

L. Ng, Response of the Aerodyne Aerosol Mass Spectrometer to Inorganic Sulfates and Organosulfur Compounds: Applications in Field and Laboratory Measurements. *Environ. Sci. Technol.* **53**, 5176–5186 (2019).

17. E. Dovrou, C. Y. Lim, M. R. Canagaratna, J. H. Kroll, D. R. Worsnop, F. N. Keutsch, Measurement techniques for identifying and quantifying hydroxymethanesulfonate (HMS) in an aqueous matrix and particulate matter using aerosol mass spectrometry and ion chromatography. *Atmospheric Meas. Tech.* **12**, 5303–5315 (2019).

18. P. F. DeCarlo, J. R. Kimmel, A. Trimborn, M. J. Northway, J. T. Jayne, A. C. Aiken, M. Gonin, K. Fuhrer, T. Horvath, K. S. Docherty, D. R. Worsnop, J. L. Jimenez, Field-deployable, high-resolution, time-of-flight aerosol mass spectrometer. *Anal. Chem.* **78**, 8281–8289 (2006).

19. P. F. DeCarlo, J. G. Slowik, D. R. Worsnop, P. Davidovits, J. L. Jimenez, Particle Morphology and Density Characterization by Combined Mobility and Aerodynamic Diameter Measurements. Part 1: Theory. *Aerosol Sci. Technol.* **38**, 1185–1205 (2004).

20. J. M. St. Clair, A. K. Swanson, S. A. Bailey, G. M. Wolfe, J. E. Marrero, L. T. Iraci, J. G. Hagopian, T. F. Hanisco, A new non-resonant laser-induced fluorescence instrument for the airborne in situ measurement of formaldehyde. *Atmospheric Meas. Tech.* **10**, 4833–4844 (2017).

21. J. M. St. Clair, A. K. Swanson, S. A. Bailey, T. F. Hanisco, CAFE: a new, improved nonresonant laser-induced fluorescence instrument for airborne in situ measurement of formaldehyde. *Atmospheric Meas. Tech.* **12**, 4581–4590 (2019).

22. L. Zeng, A. P. Sullivan, R. A. Washenfelder, J. Dibb, E. Scheuer, T. L. Campos, J. M. Katich, E. Levin, M. A. Robinson, R. J. Weber, Assessment of online water-soluble brown carbon measuring systems for aircraft sampling. *Atmospheric Meas. Tech.* **14**, 6357–6378 (2021).

23. Y. Yang, M. A. Battaglia, M. K. Mohan, E. S. Robinson, P. F. DeCarlo, K. C. Edwards, T. Fang, S. Kapur, M. Shiraiwa, M. Cesler-Maloney, W. R. Simpson, J. R. Campbell, A. Nenes, J. Mao, R. J. Weber, Assessing the Oxidative Potential of Outdoor PM2.5 in Wintertime Fairbanks, Alaska. *ACS EST Air*, doi: 10.1021/acsestair.3c00066 (2024).

24. S. Albertin, S. Bekki, J. Savarino, N. Brett, K. S. Law, M. Cesler-Maloney, J. H. Flynn, F. Guo, B. Barret, N. Caillon, B. D'Anna, E. Dieudonné, A. Lamothe, S. Richard, B. Temime-Roussel, B. Alexander, S. R. Arnold, S. Decesari, G. J. Fochesatto, J. Mao, W. Simpson, Unraveling Urban NO Emission Sources in Polluted Arctic Wintertime Using NO2 Nitrogen Isotopes. *J. Geophys. Res. Atmospheres* **129**, e2024JD041842 (2024).

25. K. C. Nattinger, TEMPORAL AND SPATIAL TRENDS OF FINE PARTICULATE MATTER COMPOSITION IN FAIRBANKS, ALASKA. 144 (2016).

26. T. M. Olson, M. R. Hoffmann, Hydroxyalkylsulfonate formation: Its role as a S(IV) reservoir in atmospheric water droplets. *Atmospheric Environ. 1967* **23**, 985–997 (1989).

27. E. S. Robinson, M. Cesler-Maloney, X. Tan, J. Mao, W. Simpson, P. F. DeCarlo, Wintertime spatial patterns of particulate matter in Fairbanks, AK during ALPACA 2022. *Environ. Sci. Atmospheres*, doi: 10.1039/D2EA00140C (2023).

28. S. Guo, M. Hu, M. L. Zamora, J. Peng, D. Shang, J. Zheng, Z. Du, Z. Wu, M. Shao, L. Zeng, M. J. Molina, R. Zhang, Elucidating severe urban haze formation in China. *Proc. Natl. Acad. Sci.* **111**, 17373–17378 (2014).

29. W. C. Hinds, Y. Zhu, *Aerosol Technology: Properties, Behavior, and Measurement of Airborne Particles* (John Wiley & Sons, 2022; https://books.google.com/books?hl=en&lr=&id=p8p6EAAAQBAJ&oi=fnd&pg=PR11&dq=Aerosol+Technology:+Properties,+Behavior,+and+Measurement+of+Airborne+Particles,+3rd+Edition,&ots=4Nj1AttWYu&sig=P_ylSEyecIYPLe4hdhMrFOWUifI).

30. I. Riipinen, J. R. Pierce, T. Yli-Juuti, T. Nieminen, S. Häkkinen, M. Ehn, H. Junninen, K. Lehtipalo, T. Petäjä, J. Slowik, R. Chang, N. C. Shantz, J. Abbatt, W. R. Leaitch, V.-M. Kerminen, D. R. Worsnop, S. N. Pandis, N. M. Donahue, M. Kulmala, Organic condensation: a vital link connecting aerosol formation to cloud condensation nuclei (CCN) concentrations. *Atmospheric Chem. Phys.* **11**, 3865–3878 (2011).

31. E. Dovrou, K. H. Bates, J. M. Moch, L. J. Mickley, D. J. Jacob, F. N. Keutsch, Catalytic role of formaldehyde in particulate matter formation. *Proc. Natl. Acad. Sci.* **119**, e2113265119 (2022).

32. J. M. Moch, E. Dovrou, L. J. Mickley, F. N. Keutsch, Y. Cheng, D. J. Jacob, J. Jiang, M. Li, J. W. Munger, X. Qiao, Q. Zhang, Contribution of Hydroxymethane Sulfonate to Ambient Particulate Matter: A Potential Explanation for High Particulate Sulfur During Severe Winter Haze in Beijing. *Geophys. Res. Lett.* **45** (2018).

Gas and meteorological measurements at the CTC site in Fairbanks, Alaska, during the ALPACA-2022 field study can be found at https://doi.org/10.18739/A27D2Q87W.

AMS-Sulfate, nitrate, ammonium, organic aerosols and PILS-S(IV) measurements can be found at https://doi.org/10.18739/A2WP9T83H .

The data portal can be accessed at https://arcticdata.io/catalog/portals/ALPACA .